JOURNAL OF MATERIALS SCIENCE 30 (1995) 2401–2405

Optimization of interfacial bonding to enhance fracture toughness of ceramic matrix reinforced with metallic ribbon

T. K. LEE, K. N. SUBRAMANIAN
Department of Materials Science and Mechanics, Michigan State University, East Lansing, MI 48824, USA

The role of interface on the fracture toughness of ceramic glass reinforced with metallic ribbon was investigated. A strong interfacial bonding strength is essential for load transfer between the matrix and ribbon, and for utilization of the ductility of the reinforcement. However, weak interfacial bonding is considered to be important so that ribbon pull-out can improve the toughness of brittle ceramic matrix composites. The main aim of the present study is to carry out interface design to optimize mechanical properties of brittle ceramic matrix composites reinforced with ductile metallic ribbons.

1. Introduction

Various studies on fracture toughness and interfacial bonding in a ceramic matrix reinforced with ceramic fibres have shown that high fracture toughness can be obtained in ceramic matrix composites that possess weak interfacial bonding [1–12]. A major mechanism of enhancement of fracture toughness in such composite systems is the bridging of crack surfaces by intact fibres. This involves frictional sliding of fibres against the matrix following interfacial debonding and failure of the fibres. It requires weak interfacial bonding between the reinforcements and the matrix. On the other hand, ceramic matrix composites containing metallic reinforcements strongly bonded to the matrix have exhibited profoundly high fracture toughness [13–20]. The work done during plastic deformation of the metallic reinforcements between the crack surfaces in the bridging zone contributes to the overall toughness of these composites. Therefore, if both plastic deformation of the reinforcement and frictional sliding between the components can be utilized in the same composite, the fracture toughness of the ceramic matrix composite with metallic reinforcement may be significantly improved. Since such contributions are controlled by the interfacial bonding strength between the matrix and the reinforcement, maximum fracture toughness can be achieved by modification of interfacial characteristics.

Thermal cycling [21] and acid etching [22] techniques have been recently reported for modification of interfaces in soda–lime–silica glass matrix composites reinforced with Nichrome ribbon. With continued thermal cycling, interfacial microcracks due to thermal expansion mismatch between the constituents accumulate at the interface, resulting in weaker interfacial bonding. On the other hand, the ribbon surface roughened by acid etching prior to composite fabrication provides a jagged interface for the composite. As a result, mechanical interlocking at the jagged interface leads to strong interfacial bonding.

Although several researchers have reported that fibre-reinforced ceramic composites exhibit a dramatic improvement in toughness compared with monolithic ceramics [2, 3, 13], their choice of critical stress intensity factor, K_{Ic}, or critical energy release rate, J_{Ic}, as a material property are questionable for these composites [23, 24]. As a matter of fact, a meaningful technique to evaluate the fracture toughness as a material property for such a system is not yet established, due to the difficulty in defining representative characteristics of crack propagation, such as crack front deflection, crack wake delamination and crack bridging. Especially in ceramic matrix composites containing ductile reinforcements, plastic deformation of the reinforcements adds to such difficulty. Recently, Ashby proposed a method to estimate upper and lower limits for toughness, J_{Ic}, for such composites based on a postulated "best" and "worst" case [24]. However, most of the studies dealing with fracture toughness enhancement due to crack bridging in ceramic matrix composites containing ductile reinforcements use the following equation [14–17]

$$\Delta G_c = V_f \int_0^{u^*} \sigma(u)\, du \qquad (1)$$

where V_f is the area fraction of reinforcement intercepted by the crack, $\sigma(u)$ is the normal stress acting on the reinforcement, and u^* is the crack opening at the point where reinforcement fails. This equation is derived on the basis of J-integral analysis [5], which is not applicable to such composites. However, the resultant equation itself represents the strain energy release rate enhancement due to crack bridging by intact reinforcements. Therefore, the value obtained from this

0022–2461

equation is adopted as the toughness increment due to crack bridging in the ceramic composite in this study, although it is not considered as a material property.

The principal aim of the present study is to elucidate interfacial effects on mechanical properties of the brittle matrix with ductile reinforcement, and finally to control the interfacial bonding strength in order to obtain optimum mechanical properties for the composite. Ribbon geometry of the reinforcement was selected in this study to facilitate ease of fabrication and theoretical modelling of the composite.

2. Experimental procedure

The composite material used in this study was a soda–lime–silica glass matrix composite reinforced with a single Nichrome (80 wt %Ni–20 wt %Cr) ribbon. The composite was fabricated by sandwiching a series of ribbons (1.8 mm wide and 80 μm thick) between glass slides, and curing at 710 °C for 3 h in air. The mechanical and physical properties of the matrix and ribbon are listed in Table I.

In order to obtain the various interfacial characteristics of the composites, thermal cycling and acid etching techniques were used in the present study. The details of these techniques have been reported in previous papers [21, 22]. In this paper, the composite specimens that have undergone three and seven thermal cycles between room temperature and 650 °C are referred to as TC-3, and TC-7, respectively. AE-60 and AE-90 are used to refer to 60 and 90s acid etched ribbons in as-received conditions, and PAE refers to 60 s acid etched ribbons in preoxidized conditions. Etching was carried out with 20% HNO_3 and 80% HCl solution. NT is used to denote composites with ribbons in as-received condition.

The fracture toughness behaviour of the composite was characterized by flexure and tension tests. A three point bending test with a span of 18 mm was carried out using a single notched beam (5 mm wide and 6 mm thick). The length of the sample was varied from 20 to 30 mm. Using values of the peak load obtained from the three point bending test, K_{Ic} was calculated based on the linear elastic fracture mechanics analysis [25]. As soon as the matrix was cracked (as observed by the load drop), the specimen was unloaded. Due to such a procedure, the specimen contained a circumferential crack around the Nichrome ribbon, as shown in Fig. 1. Tension tests were carried out with these precracked specimens, in order to characterize the bridging effect on the fracture toughness of the composite. The precracked specimens were placed carefully in a specially designed selfaligning fixture. For effective gripping, the glass part of the specimen was held by glass fibre reinforced epoxy which was glued to the fixture. The stress–displacement curves were recorded, using a computer controlled Instron testing machine at a crosshead speed of 0.2 mm min^{-1}. The areas under the curves were measured and the values of the fracture toughness due to crack bridging were calculated. Fractographic observations were made on the specimens fractured during tensile loading, using an Olympus stereo optical microscope.

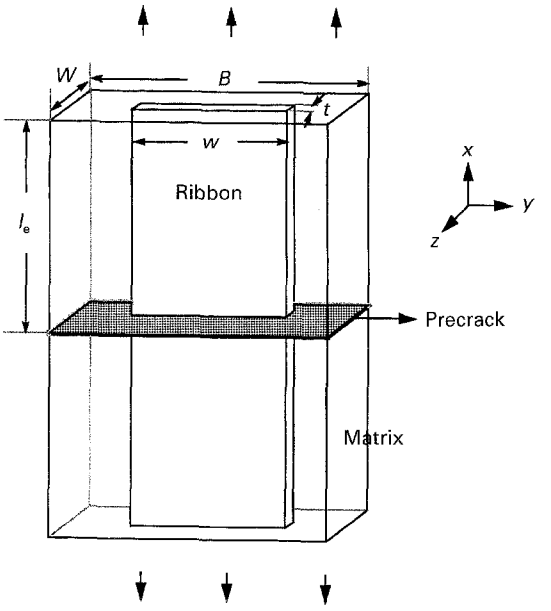

Figure 1 A schematic sketch of a precracked sample used in tension tests to evaluate fracture toughness due to crack bridging, ΔG_c. $B = 6.0$ mm, $W = 5.0$ mm, $w = 1.8$ mm, $t = 80$ μm. l_e is variable.

TABLE I Physical and mechanical properties of constituents of the composite

	Matrix	Ribbon
Material	Soda–lime slide glass	Nichrome
Thermal expansion coefficient 10^{-6} °C^{-1},(25–500 °C)	9.2	14.3
Young's modulus, GPa	72	213
Yield strength, MPa		305
Tensile strength, MPa		700
Softening temperature, °C	700	

3. Results and discussion

3.1. Fracture toughness, K_{Ic}, behaviour

The calculated fracture toughness, K_{Ic}, values of soda–lime glass matrix composites reinforced with Nichrome ribbons in various interfacial bonding conditions are given in Table II. The interfacial bonding conditions utilized were as follows:

1. The specimens which were subjected to thermal cycling had weak interfacial bonding conditions. Moreover, it is important to note that as the number

TABLE II Fracture toughness, K_{Ic}, of Nichrome ribbon reinforced soda–lime glass matrix with various bonding conditions

Bonding conditions	Reinforcement (vol %)	K_{Ic} MPa $m^{1/2}$
Matrix	0.0	0.98 ± 0.05
NT	0.8	1.16 ± 0.09
TC-3	0.5	1.22 ± 0.11
TC-7	0.5	1.17 ± 0.16
AE-60	0.5	1.11 ± 0.04
PAE-60	0.5	1.17 ± 0.09

of thermal cycles increased, the interfacial bonding strength decreased [21].

2. The composite specimens reinforced with acid etched Nichrome ribbon showed strong interfacial bonding due to mechanical interlocking along the interface. This mechanical interlocking effect was lower in the composite with ribbons that were pre-oxidized prior to acid etching [22].

Regardless of the interfacial bonding condition, an increase of up to 20% in fracture toughness was achieved for composites with 0.5 vol % reinforcement. Prestressing of the matrix due to the differential thermal expansion coefficient between the matrix and ribbon and crack shielding by the ribbons may be attributed to the enhancement in fracture toughness, K_{Ic}, of the present composite system. Since the thermal expansion coefficient of the ribbon is larger than that of the glass matrix, the matrix is in compression along the direction parallel to the length of the ribbon, thus providing a compressive zone which increases the level of applied stress required to open the crack [8, 26, 27]. Crack shielding by the ribbon impedes the crack propagation and also changes the crack front configuration [26, 28, 29]. Fractographic evidence of the crack shielding by the ribbon is shown in Fig. 2. The interference fringes represent the path of the crack. Fig. 2 clearly shows that the ribbon impedes the motion of the crack as it crosses the ribbon. As described by Green *et al.* [28], the crack is pinned at both the edges of the ribbon, resulting in crack bowing. Following crack bowing, the secondary crack initiates behind the ribbon and propagates fast to catch up with the primary crack.

However, the interfacial debonding process, which has been reported as a major mechanism of fracture toughness enhancement in fibre reinforced ceramic matrix composites, was not observed during matrix cracking in the case of the present system. Catastrophic matrix failure, due to considerably low volume fraction of the ribbon in the composites, leads to negligible interfacial debonding during flexural loading.

3.2. Tensile behaviour of precracked composite

Typical stress–displacement curves (with nominal stress referring to load per unit ribbon cross-sectional area) obtained from the tensile tests on the precracked composite specimens with various interfacial bonding conditions are given in Fig. 3. The results given in Fig. 3 are for composites reinforced with a ribbon of 12 mm embedded length, l_e, (defined in Fig. 1). In the AE specimen (the strongest bonding condition) the ribbon fractured at a considerably small displacement, curve A. As the bonding became weaker, the ribbon fractured at larger displacements as seen in curve B for the non-treated composite specimen. The "gauge length" of the ribbon is confined to the debonded length along the embedded ribbon. Also, the debonded length decreases with an increase in interfacial bonding strength of the composite for a given applied stress. As a result, a general trend, in spite of some inconsistencies, indicating that the displacement at the point where the ribbon fractured decreased with an increase in the interfacial bonding strength, can be noted in the data provided in Table III. On the other

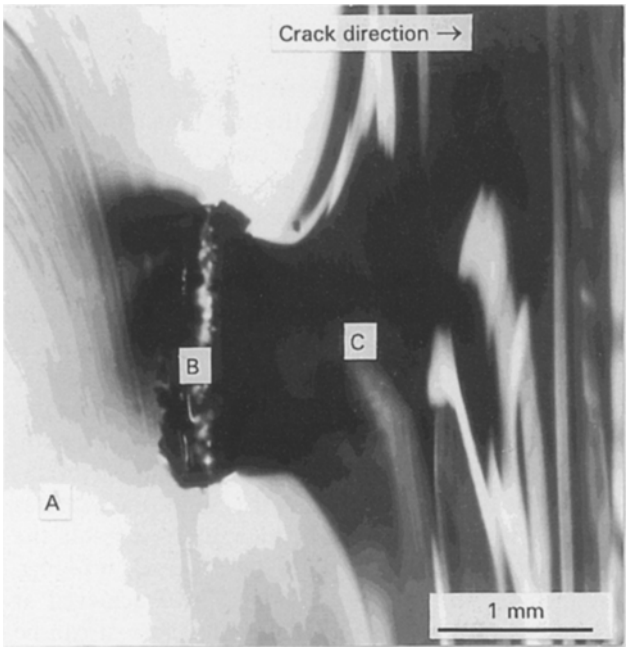

Figure 2 Fractographic observation of crack shielding by the ribbon. Interference fringes represent the path of the crack: (A) primary crack plane, (B) ribbon, (C) secondary crack plane.

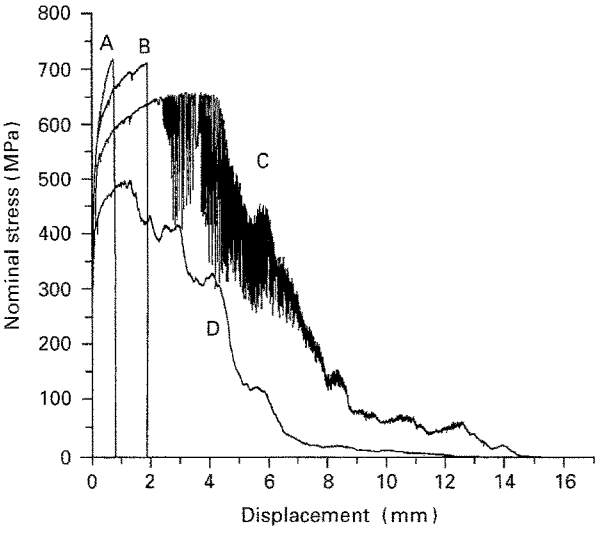

Figure 3 Typical stress–displacement curves obtained from the tensile loading of precracked composite specimens with various interfacial bonding conditions: (A) AE, (B) NT, (C) TC-3, and (D) TC-7.

TABLE III Effect of interfacial bonding on displacement at the ribbon fracture

Bonding condition	AE-60	PAE-60	AE-60	NT	TC-3	TC-7
Displacement at ribbon fracture (mm)	0.67 ± 0.05	0.85 ± 0.28	1.02	1.64 ± 0.50	1.63 ± 0.58	1.48 ± 0.24

hand, the ribbon pull-out from the matrix after complete debonding was observed in TC-3 and TC-7 specimens (curves C and D, respectively). However, there was noticeable difference between these two cases. For TC-3 specimens, the interfacial bonding was strong enough to prevent complete debonding of the ribbon during initial stages of the test. As a result, the effective length of the bonded portion of the ribbon was large enough to sustain considerable plastic deformation, before complete debonding occurred. On the other hand, in the TC-7 specimens containing mostly interconnected microcracks, the interfacial bonding was so weak that the debonding crack propagated more easily along the interface as compared to the TC-3 specimen. In addition to this, the low static frictional shear stress at the debonded interface (in TC-7) was not effective enough to hold the debonded portion of the ribbon. Therefore, complete debonding occurred at a much lower stress than that of the TC-3 specimen [21]. Hence, the extent of plastic deformation was very low in the case of the TC-7 specimens. However, the displacement at a given stress level was considerably large when compared to that of the TC-3 specimen because of the difference in the debonded length, "gauge length", of the ribbon between both cases.

The heavy shaded portion observed in the case of the TC-3 specimen (Fig. 3) indicates the "stick–slip" friction phenomenon. In this portion of the curve, each load drop was accompanied by an audible "click". The mechanism of this phenomenon has been explained by Griffin *et al.* [30] and Deshmukh *et al.* [31]. According to Griffin *et al.*, Poisson's contraction and expansion of the fibre, in combination with a difference between static and dynamic friction, leads to stick–slip friction. In contrast, Deshmukh *et al.* pointed out that the release of excess strain energy stored in the free length of the fibre when the fibre is reloaded contributes to the above phenomenon. As illustrated in curve C, the stress amplitude and wavelength of the stick–slip behaviour decreases as the ribbon is progressively pulled out. This can be explained by the smoothening effect of the debonded interface during ribbon pull-out, since such a behaviour predominantly depends on the asperities of the debonded surfaces at the interface. The stick–slip behaviour was not observed in the TC-7 specimens due to the smooth feature of the debonded interface, resulting in low frictional shear stress [21].

3.3. Toughness due to crack bridging, ΔG_c

Fracture toughness due to crack bridging, ΔG_c, of the composite in various bonding conditions was evaluated using Equation 1 and the area under the curves. The results are given in Table IV. For cases with ribbon fracture (curves A and B in Fig. 3), the area under the curves was considerably smaller when compared to that of the area under curve C, which consists of contributions from both plastic deformation and frictional sliding of the ribbon. It is apparent from these curves that the stronger the interfacial bonding, the smaller the area under the curve, due to the small displacement at ribbon fracture. Even though both curves C and D are comprised of plastic deformation and frictional sliding stages, the total area under curve D is much smaller than that of curve C, because of the low plastic deformation and low frictional shear stress involved in curve D. From these observations, it can be inferred that the TC-3 specimen, with a 11 mm embedded length of ribbon shows a maximum fracture toughness due to crack bridging, ΔG_c. In addition, the effect of the embedded ribbon length on toughness of non-treated composite specimens is shown in Fig. 4. The ribbon fractured in the composite, with over 12 mm embedded ribbon length; while ribbon pull-out occurred after plastic deformation of the debonded ribbon in the composite with less than 11 mm embedded ribbon length. As a result, the maximum fracture toughness due to crack bridging, ΔG_c, in the non-treated composite was achieved at 11 mm embedded ribbon length. Therefore, it can be defined as the "critical embedded length", l_{cr}, for the maximum fracture toughness due to crack bridging in a given bonding condition (and for a given ribbon thickness) since a ribbon with this length effectively undergoes both plastic deformation and frictional sliding phenomena. The critical embedded length in various bonding conditions is shown in Table V. Due to the wide variation in data, the results are presented as a range, instead of a single value. Nevertheless, it can be concluded from the results of this study that the

TABLE IV Fracture toughness due to crack bridging, ΔG_c, in various bonding conditions. $\Delta G_c = V_f \times$ area under the stress–displacement curve in Fig. 3

	ΔG_c(kJ m^{-2})		
	Plastic deformation	Frictional sliding	Total
NT	6.08	0.00	6.08
AE-60	2.87	0.00	2.87
TC-3	7.03	13.48	20.51
TC-7	3.25	7.67	10.92

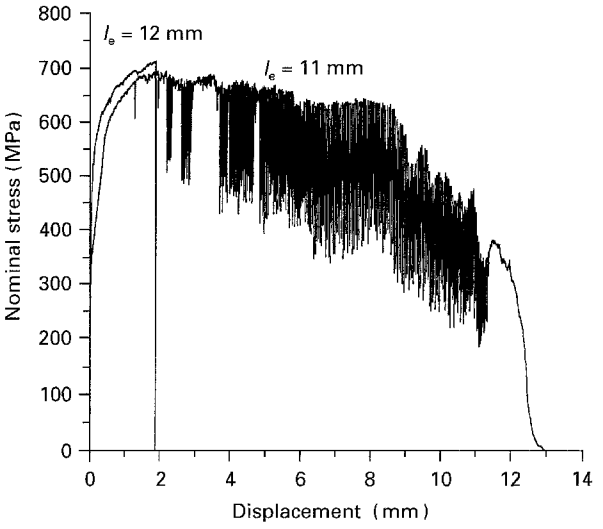

Figure 4 Stress–displacement curves showing the effect of the embedded ribbon length on toughness, ΔG_c, of NT composite specimens.

TABLE V Critical embedded length l_e, for the maximum fracture toughness due to crack bridging in various bonding conditions

Bonding conditions	NT	AE-60	PAE-60	TC-3	TC-7
Critical embedded length (mm)	10–12	< 3	< 3	10–13	15–17

maximum fracture toughness due to crack bridging can be achieved by using discontinuous metallic reinforcements with a length less than or equal to the critical embedded length in the ceramic matrix composites.

4. Conclusions

1. An increase of up to 20% in fracture toughness, K_{Ic}, was achieved in the composite used in the present study, due to "prestressing" in the matrix and "crack shielding" by the ribbon.

2. Introduction of even a very low volume fraction of metallic ribbon provides significant improvement in fracture toughness due to crack bridging, ΔG_c, in the brittle glass matrix.

3. To obtain maximum toughness in these composites, it is essential to retain the optimum bonding strength.

4. The results of this study suggest that the enhancement in toughness may be achieved by using discontinuous metallic ribbon reinforcements in the brittle ceramic matrix, $l_e \leq l_{cr}$.

Acknowledgements

The authors acknowledge the Composite Materials and Structures Center at Michigan State University for supporting this project.

References

1. D. C. PHILLIPS, *J. Mater. Sci.* **9** (1974) 1847.
2. K. M. PREWO and J. J. BRENNEN, *ibid.* **15** (1980) 463.
3. J. BRENNEN and K. PREWO, *ibid.* **17** (1982) 2371.
4. K. M. PREWO and J. J. BRENNEN, *ibid.* **17** (1982) 1201.
5. A. G. EVANS and R. M. McMEEKING, *Acta Metall.* **34** (1986) 2435.
6. M. D. THOULESS and A. G. EVANS, *ibid.* **36** (1988) 517.
7. B. BUDIANSKY, J. C. AMAZIGO and A. G. EVANS, *J. Mech. Phys. Solids* **36** (1988) 167.
8. A. G. EVANS and D. B. MARSHALL, *Acta Metall.* **37** (1989) 2567.
9. A. G. EVANS, *Mater. Sci. Eng.* **A107** (1989) 227.
10. L. S. SIGL and A. G. EVANS, *Mech. Mater.* **8** (1989) 1.
11. A. G. EVANS, *J. Amer. Ceram. Soc.* **73** (1990) 187.
12. S. V. NAIR, *ibid.* **73** (1990) 2839.
13. V. D. KRSTIC, P. S. NICHOLSON and R. G. HOAGLAND, *ibid.* **64** (1981) 499.
14. L. S. SIGL, P. A. MATAGA, B. J. DALGEISH, R. M. McMEEKING and A. G. EVANS, *Acta Metall.* **36** (1988) 945.
15. M. F. ASHBY, F. J. BLUNT and M. BANNISTER, *ibid.* **37** (1989) 1847.
16. H. E. DÈVE, A. G. EVANS, G. R. ODETTE, R. MEHRABIAN, M. L. EMILIANI and R. J. HECHT, *Acta Metall. Mater.* **38** (1990) 1491.
17. G. BARAN, M. DEGRANGE, C. ROQUES-CARMES and D. WEHBI, *J. Mater. Sci.* **25** (1990) 4211.
18. K. S. RAVICHADRAN, *Acta Metall. Mater.* **40** (1992) 1009.
19. F. E. HEREDIA, M. Y. HE, G. E. LUCAS, A. G. EVANS, H. E. DÈVE and D. KONITZER, *ibid.* **41** (1993) 505.
20. T. K. LEE and K. N. SUBRAMANIAN, *J. Mater. Sci. Lett.* **12** (1993) 1758.
21. *Idem, Scripta Metall. Mater.* **28** (1993) 1405.
22. *Idem, ibid.* **30** (1994) 159.
23. D. B. MARSHALL and A. G. EVANS, *J. Amer. Ceram. Soc.* **68** (1985) 225.
24. M. F. ASHBY, *Acta Metall. Mater.* **41** (1993) 1313.
25. W. F. BROWN, JR and J. E. SLAWLEY, *ASTM STP* 410 (American Society Testing Materials, Philadelphia, 1966) p. 1.
26. R. W. RICE, *Ceram. Eng. Sci. Proc.* **2** (1981) 661.
27. R. L. LEHMAN and C. A. DOUGHAN, *Comp. Sci. Technol.* **37** (1990) 149.
28. D. J. GREEN, P. S. NICHOLSON and J. D. EMBURY, *J. Mater. Sci.* **14** (1979) 1413.
29. R. U. VAIDYA and K. N. SUBRAMANIAN, *ibid.* **25** (1990) 3291.
30. C. W. GRIFFIN, S. Y. LIMAYE, D. W. RICHERSON and D. K. SHETTY, *Ceram. Eng. Sci. Proc.* **9** (1988) 671.
31. U. V. DESHMUKH and T. W. COYLE, *ibid.* **9** (1988) 627.

Received 11 August 1993
and accepted 8 September 1994